

This is the peer reviewed version of the following article: *Journal of Applied Polymer Science*, 138(20), 50425. 2021, which has been published in final form at <https://doi.org/10.1002/app.50425>. This article may be used for non-commercial purposes in accordance with Wiley Terms and Conditions for Use of Self-Archived Versions.

---

## **Effect of the Elastomer Viscosity on the Morphology and Impact Behavior of Injection Molded Foams Based on blends of Polypropylene and Polyolefin Elastomers**

Santiago Muñoz-Pascual<sup>1,\*</sup>, Cristina Saiz-Arroyo<sup>2</sup>, Anja Vananroye<sup>3</sup>, Paula Moldenaers<sup>3</sup> and Miguel Angel Rodriguez-Perez<sup>1</sup>

1 Cellular Laboratory (CellMat), University of Valladolid, Valladolid 47011, Spain\*

2 CellMat Technologies S.L., Paseo de Belen 9-A (Parque Científico-UVa Building), 47011, Valladolid, Spain

3 Soft Matter Rheology and Technology, Department of Chemical Engineering, KU Leuven, Celestijnenlaan 200F, Box 2424, B-3001 Leuven, Belgium

Correspondence to: [santiagomp@fmc.uva.es](mailto:santiagomp@fmc.uva.es);

### **ABSTRACT**

The impact resistance of injection-molded polypropylene (PP) parts is severely reduced when they are foamed. It is necessary to implement strategies, such as elastomer toughening, to increase the impact behavior of foamed parts. However, the knowledge on the effect of elastomer addition on the morphology, cellular structure and impact of injection-molded cellular parts is very limited. In this work, foamed parts based on blends of PP and polyolefin elastomers (POE) have been produced and characterized. A high and a low viscosity octene-ethylene copolymer (EOC) and a high viscosity butene-ethylene copolymer (EBC) were employed. The blends have been thermally and rheological characterized. Solids materials and foams (relative density 0.76) were injection-molded. The solid phase and cellular structure morphologies were studied using SEM. The results showed that elastomer toughening has been successful to obtain an improvement of the impact behavior in solid and cellular polymers. In this case, EOC materials provide an appropriate interfacial adhesion and optimized cellular structure which results in high impact resistance. The optimum elastomer to improve the properties is the EOC with a higher viscosity which provides impact resistance with  $n$  values below 3 due to the toughening of polymer matrix, thick skin thickness and low cell size.

### **INTRODUCTION**

Polypropylene (PP) is one of the most used thermoplastics. This is due to its low cost and excellent properties. Some of these properties are low density, processing stability, easy recycling, moisture resistance, high thermal stability, and excellent chemical and corrosion resistance. However, the use of PP in structural applications is limited by its limited impact strength.<sup>1-3</sup> There are two common approaches to improve the impact strength of PP: the use of physical blends with elastomers or the synthesis of PP

copolymers. Physical blending with elastomers allows a complete and easier characterization of the components and facilitates a proper understanding of the effect of the dispersed phase on the final properties. In addition, physical blending gives a lot of freedom from an applied point of view and a very interesting system to analyze from an academic point of view. Finally, using this approach, it is possible to design blends that could fulfill several requirements at the same time (adequate viscosity for injection molding, good foamability, high impact strength, etc.) For all these reasons, we have focused our attention on this strategy instead of using as raw materials PP copolymers.

Poly(styrene–ethylene–butylene–styrene) (SEBS),<sup>2,4</sup> ethylene-propylene rubber (EPR),<sup>5,6</sup> or ethylene propylene–diene monomer elastomer (EPDM)<sup>1,7</sup> are some of the most used impact modifiers in PP. One of the most promising elastomer groups is ethylene/ $\alpha$ -olefin copolymers or polyolefin elastomers (TPO or POE). Included in this group, ethylene-octene copolymers (EOC) can provide properties such as good shear thinning behavior, melt elasticity, and melt processability.<sup>8</sup> Ethylene-butene copolymers have been used in a lower extend but, they have also been reported as impact modifiers for PP.<sup>9,10</sup>

The importance of several factors to achieve the elastomer toughening in solid (non-cellular) PP based materials has been widely reported, such as the processing method, the nature of the matrix (crystallization, glass transition temperature, etc), the content of the elastomer the interfacial adhesion between polymer matrix and elastomer.<sup>11,12</sup> One of the most determining parameters is the distance between elastomer particles, which depends on the elastomer particles' size. It is known that the reduction of the droplet diameter, diminishing the interparticle distance, causes an increment in the impact response of the blend.<sup>12-16</sup> In the case of PP/EOC blends, this result has been reported by Premphet et al..<sup>16</sup>

The morphology and microstructure of polymer blends strongly depend on the processing method. It exists a clear relation between the microstructure of a blend and the process conditions through rheology. Capillarity number (Ca) states this relation.<sup>17</sup> Assuming a dispersion of two immiscible fluids, this number expresses the resistance of a dispersed droplet to be deformed (Equation 1):<sup>17</sup>

$$Ca = \frac{\eta_m \dot{\gamma} R}{\sigma} \quad (1)$$

Where  $\eta_m$  is the viscosity of the matrix,  $\dot{\gamma}$  the shear rate at which the blend supports,  $R$  is the radius of the droplet, and  $\sigma$  the interfacial tension between the phases. When a polymer blend is extruded or mixed, the dispersed phase is exposed to shear, and the particles can be elongated until breaking up in smaller particles. This will occur when a critical capillarity number is exceeded.<sup>18</sup> Following Wu, the critical capillarity number is:<sup>18</sup>

$$Ca_{crit} = \frac{\eta_m \dot{\gamma} R}{\sigma} = 4p^{\pm 0.84} \quad (2)$$

Where  $p$  is the ratio between the components' viscosities (Equation 3), using the solution with + for  $p > 1$  or the solution with – for  $p < 1$ .

$$p = \frac{\eta_d}{\eta_m} \quad (3)$$

With this relation, it can be concluded that to obtain a minimum droplet radius, a shear rate as high as possible must be used during processing. Also, a minimum radius is reached when the viscosity ratio is 1 (equal viscosity of the components of the blend). Then, the relation between viscosity and microstructure is given by the previous equations: Varying the elastomer viscosity, different microstructures can be produced. Shariatpanahi and Tokita have proposed similar relations to Equation 2.<sup>19, 20</sup>

Once the blend is produced the final part is obtained typically by injection molding. An important aspect to consider is that in this process, the velocity of the polymer filling the mold is not constant. Thus, a shear rate gradient is present, producing a hierarchy morphology.<sup>21-23</sup> Apart from the shear rate, temperature also has a gradient along the mold profile. This can also affect the final elastomer morphology through coalescence and relaxation mechanisms<sup>24-27</sup>. These effects have been already analyzed in detail for solid (non-foamed) injection molded parts but not for foamed polymers.

Other key parameter that has an influence on the impact resistance is the interfacial adhesion and the compatibility between phases. An increase in the adhesion implies a drop in the interfacial tension and an increase in the interphase thickness.<sup>24</sup> In addition, the adhesion between phases is crucial.<sup>24</sup> Numerous studies have been carried out to improve the adhesion by different strategies such as the use of compatibilizers or grafted polymers.<sup>12</sup> Examples are given by Yu, Wahit or Lim in polyamide, PP and grafted POE blends<sup>8,25, 26</sup> The influence of this parameter has not been analyzed in foamed materials.

Finally, the relation between microstructure and viscosity is, in principle, given by the previous equations (Equation 1, 2 and 3). However, several publications have employed elastomers of different viscosities, obtaining unexpected results. For example, Yokohama studied PP with EOC and EBC blends of different viscosity.<sup>9</sup> High viscosity compounds offered better impact properties despite the coarser elastomer structures. They affirmed that molecular weight and chemical nature of the rubber was more important than the effect of morphology. The same effect was observed by Rabinovitch.<sup>27</sup> He attributed a higher efficiency to high viscosity EOC. Once again, these studies have been performed in solid (non-foamed) materials, but there are not previous detailed studies for cellular polymers.

The elastomer toughening strategy described previously can also be used for cellular polymers. The interest lies in the low impact performance of these materials. It is well known that the dependence on the properties of cellular materials (elastic modulus, strength, or thermal conductivity) with foam density can be modelled by scaling law models, as equation 4:<sup>28</sup>

$$X_{foam} = C \cdot X_{solid} \cdot \left(\frac{\rho_{foam}}{\rho_{solid}}\right)^n \quad (4)$$

Where  $X_{foam}$  and  $X_{solid}$  are the values of the property under consideration in the foamed and solid respectively,  $\rho_{foam}$  is the density of the foam and  $\rho_{solid}$  is the density of the solid sample.  $C$  is a constant, with values close to 1 and  $n$  reaches values between 1 and 4, depending on the cellular structure and the considered property (for example,  $n$  is between 1 and 2 for the elastic modulus). Higher exponents imply an abrupt property decrease with the reduction of density. One example of this behavior is the impact response. For this property, exponents close to 4 have been reported,<sup>29, 30</sup> observing that even ductile

polymers can become brittle after foaming, even at high relative densities. This phenomenon known as the ductile-brittle transition is a severe drawback for the use of foams in structural applications.<sup>29, 30</sup>

Several publications have explored the use of TPO elastomers in PP injection-molded foams to enhance the impact resistance. Gong et al. studied the impact resistance of foamed and solid injection molded samples based on PP/POE blends, with EOC contents ranging from 0 wt.% to 20 wt.% at low (-80 °C) and high (20 °C) temperatures.<sup>31</sup> They discussed the elastomer morphology qualitatively. However, they did not study essential parameters such as interparticle distance or deformation of the dispersed phase. Similarly, Heidari et al. studied PP-EOC foams produced by extrusion foaming using chemical blowing agents.<sup>32</sup> The content of EOC was increased, modifying the cell morphology. Better impact resistance was obtained for higher POE contents, and besides, better cellular structures were detected. The elastomer morphology was observed but not analyzed in detail. Another related study was carried out by Zhao et al. using PP/EPDM/talc blends.<sup>33</sup> In this case, they achieved the elastomer toughening, but they did not analyze the structure and did not compare the foamed materials with their solid counterparts. In a previous study of our research team, the effect of processing conditions on the impact resistance of solids and foams based on PP/EOC were analyzed.<sup>34</sup> The obtained results were related to the crystalline morphology, elastomer droplet size, interparticle distance and cellular structure. Therefore, the previous literature of foamed materials produced from these type of blends is still scarce and there are basic aspects that are still unknown, such as the effect of the viscosity of the elastomeric phase, the influence of the interfacial adhesion between phases, the role played by interparticle distance and cellular structure on the impact response.

Bearing the previous ideas in mind, this research was designed to deepen in the understanding of the relation between raw materials properties, the morphology of the polymer matrix and of the elastomeric phase, cellular structure and the impact response focusing our attention on the effect of viscosity of the elastomeric phase and interfacial adhesion between phases. In addition, the elastomeric phase and cellular structure, key morphological characteristics for the final properties, have been analyzed in detail.

The new knowledge gained after this research would allow to develop foamed materials with improved impact properties, and to develop strategies to avoid the ductile-brittle transition in cellular polymers produced by injection molding.

## **MATERIALS AND METHODS**

### **Materials**

The polymer matrix used is a low viscosity grade suitable for injection molding of isotactic polypropylene (iPP) ISPLEN PP080G2M, which was kindly provided by REPSOL (Spain). This material has a melt flow index of 18.5 g/10 min at 230 °C and a density of 0.905 g/cm<sup>3</sup>. Three different polyolefin elastomers from DOW were used in this study: ENGAGE 8137 (a low viscosity octene-ethylene copolymer (EOC) with a MFI of 29.78 g/10 min at 230 °C and a density of 0.864 g/cm<sup>3</sup>), ENGAGE 8150 (a high viscosity EOC with a MFI of 1.07 g/10 min at 230 °C and a density of 0.868 g/cm<sup>3</sup>) and ENGAGE HM7387 (a high viscosity ethylene-butene copolymer (EBC) with a MFI of 0.32 g/10 min at 230 °C and a density of 0.87 g/cm<sup>3</sup>). The different

levels of viscosity (high or low) were labelled by the letters L and H, being the elastomers named as EOC-L (ENGAGE 8137), EOC-H (ENGAGE 8150) and EBC-H (ENGAGE HM7387). The main properties of these elastomers are summarized in table 1.

TABLE 1. Characteristics of the elastomers

|       | Melt Flow Index<br>(230°C/2.16kg) | Tensile Modulus<br>(100% secant)<br>(MPa) | Strength at Break<br>(MPa) | Elongation at Break<br>(%) | Flexural Modulus<br>(1% secant)<br>(MPa) |
|-------|-----------------------------------|---|----------------------------|----------------------------|--|
| EOC-L | 29.78                             | 1.80                                      | 2.40                       | 800                        | 7.80                                     |
| EOC-H | 1.07                              | 2.60                                      | 9.50                       | 810                        | 15.2                                     |
| EBR-H | 0.32                              | 2.90                                      | 9.10                       | 810                        | 12.2                                     |

The blowing agent used was Hydrocerol BIH 40 provided by Clariant. It is an endothermic blowing agent composed of sodium bicarbonate and citric acid. Antioxidants Irgafos 168 (from Ciba) in a proportion of 0.08 wt.% and Irganox 1010 (from Ciba) in a proportion of 0.02 wt.% were added to the formulations to prevent thermal oxidation of the polymers during blending and injection molding.

## Experimental methods

### *Sample production*

Firstly, PP, the elastomer pellets and the antioxidants mentioned above were mixed and blended in a twin-screw extruder (Collin Teach Line model ZK 25T SCD 15). The temperature profile was 145, 150, 155, 160, and 165 °C from the hopper to the die and the screw speed was 200 rpm. At these conditions, the shear rate during the extrusion process was the maximum that the extrusion machine could offer to obtain a small particle size of the elastomeric phase (Equation 2). The elastomer content was 20 wt.% for all the blends. The pure PP and elastomers were also extruded under the same conditions used for the blends in order to compare materials with the same thermomechanical history and study all the materials (components and blends) under the same conditions. This aspect is relevant for the rheological characterization.

Solid and foamed materials were produced using a microinjection-molding machine (BabyPlast 6/10P). The temperature profile from the rear to the nozzle was 195 °C, 205 °C and 215 °C. The mold temperature was 30 °C. The foamed samples were produced using the so-called low-pressure foaming injection molding process.<sup>35</sup> A detailed description of this processing approach was given in our previous study.<sup>34</sup> A fixed percentage of blowing agent (2 wt.%) was added for all the samples and all foaming conditions. The

relative density of the obtained foamed samples was kept constant in a value of 0.76, meaning a density reduction of 24% compared to the solid blends. The dimensions of the solid and foamed materials were 81 x 14.50 x 4 mm.

### ***Rheological characterization***

Cylindrical samples with a thickness of 1.5 mm and a diameter of 22 mm were prepared in a hot-plate press at a temperature of 210 °C and with a pressure of 70 bars for 10 minutes (the minimum possible to avoid elastomer coalescence). In the pure elastomers, 150 °C was the chosen temperature due to their low melting point.

A strain-controlled rheometer ARES MELTS from TA Instruments was used to perform the dynamic shear tests. The operation temperature was 210 °C, using a controlled N<sub>2</sub> atmosphere. A fixed gap of 1.35 mm was used to perform the rheological measurements. In order to define the adequate linear strain range for all the rheological experiments, strain sweeps were performed for all the materials at a frequency of 10 rad/s, 210 °C, and in the range of strains between 0.01% and 70%. 10% strain was the chosen strain for the subsequent experiments. Using this value, the experiments are performed within the linear viscoelastic response of all the materials.

Next, a frequency sweep was carried out at the selected strain. The dynamic-mechanical experiments were performed over an angular frequency range of  $0.01 < \omega < 100$  rad/s, taking 5 points per decade. The linear viscoelastic properties, namely the complex viscosity  $\eta^*$  (defined as  $\eta^* = \eta' + i\eta''$ , where  $\eta'$  is the dynamic or real viscosity and  $i\eta''$  the imaginary part) and the complex modulus  $G^*$  (with its components: the storage modulus  $G'$  and the loss modulus  $G''$ ) were measured. At least three samples of each reference were measured. The standard deviation of the parameters measured was always lower than 1% of the average value.

For the analysis of the materials behavior, the viscosity ratio  $p$  for each blend was calculated from the viscosity values of the pure components. In our case, the ratio was calculated along all the ranges of frequencies, following equation 3.

In addition, the mixing rule and the Palierne fitting were used to analyze the obtained rheological data. The equations used are included in the Supplementary information.

### ***Calorimetric characterization***

Differential scanning calorimetry (DSC) measurements were conducted with a Mettler DSC 822 instrument, calibrated with indium, zinc and n-octane. The average weight of the samples was  $4.93 \pm 0.51$  mg. These experiments were performed in the blends obtained after the extrusion process. To study the melting and the crystallization of the compounds, the following heating program was chosen: Samples were heated from -120 °C to 250 °C at a heating rate of 10 °C/min under dry nitrogen atmosphere. Then,

they were cooled to -120 °C at the same rate and finally, the first heating slope was repeated, reaching 250°C at 10°C/min. As result, the influence of the previous thermal histories was eliminated after the first heating. The crystallinity degree was determined from the melting enthalpy, using equation 5:

$$\chi_c = \frac{\Delta H_f}{\Delta H_0} \times 100 \quad (5)$$

Where  $\Delta H_f$  is the melting enthalpy of the sample, and  $\Delta H_0$  is the 100% crystalline melting enthalpy reference. In the case of PP, the value of  $\Delta H_0$  is 207 J/g.<sup>36</sup>

### Structural characterization

In order to characterize the cellular structure of the foamed samples, the materials were quenched in liquid nitrogen and then fractured. The selected plane was TD-Z, and was obtained from the middle of the injected sample, as it can be seen in Figure 1. A thin layer of gold was sputtered on the fractured surface to make it conductive. The micrographs were taken using a Hitachi FlexSEM 1000 scanning electron microscope (SEM). Average cell diameter was determined using an image-processing tool based on ImageJ software.<sup>37</sup> Relevant statistical parameters such as the normalized standard deviation ( $SD/\phi$ ) of the cellular structure distribution were calculated using Equation 6.

$$\frac{SD}{\phi} = \frac{\sqrt{\sum_{i=1}^n \frac{(\phi_i - \phi)^2}{n}}}{\phi} \quad (6)$$

where  $n$  is the number of counted cells,  $\phi_i$  is the cell diameter of cell  $i$  and  $\phi$  is the average diameter of the cells. This parameter accounts for the width of the cell size distribution.

In addition, the skin thickness in the foamed materials was measured in several areas along the profile of the sample with ImageJ and the average value was obtained.

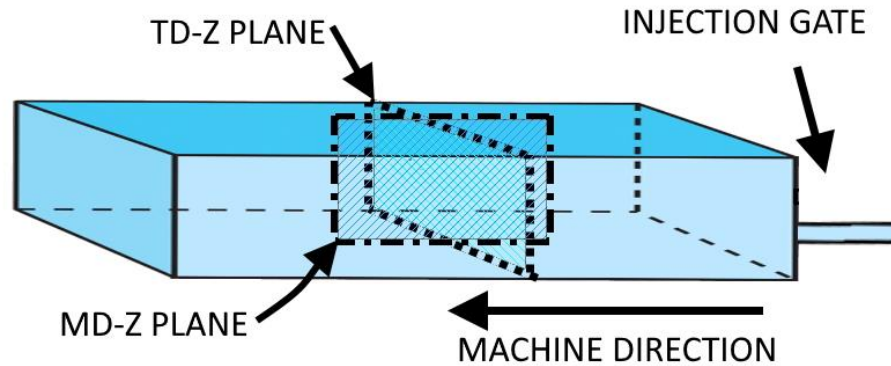


FIGURE 1. Scheme of an injection molded sample and the analyzed planes.

Elastomer phase dispersion was studied in the extruded material (before the injection,) and in the injected samples (both solid and foamed samples). To evaluate it, the specimens were quenched in liquid nitrogen and then fractured. In the case of the pre-injected material, the samples were filaments. In the injection molded samples, the fractured plane was MD-Z, due to the interest in the structure developed in this plane, following other similar studies.<sup>21-23</sup> The analyzed plane was obtained from the center of the sample,

as can be seen in figure 1. The resulting surface was etched with xylene at room temperature for 15 hours to remove the elastomer phase from the PP matrix. Subsequently, gold was sputtered on the surface, and SEM images were taken. In the case of the injected samples, images were taken for the following distance from the skin: 50, 100, 200, 500, 1000 and 2000  $\mu\text{m}$ . Using ImageJ software, the particle area, the major axis and the long and short axis were measured. The equivalent diameter of each particle was calculated from area, and the number average ( $D_n$ ) and volume average diameter ( $D_v$ ) of the distribution were calculated using equations 7 and 8 respectively:

$$D_n = \frac{\sum N_i D_i}{\sum N_i} \quad (7)$$

$$D_v = \frac{\sum N_i D_i^4}{\sum N_i D_i^3} \quad (8)$$

Where  $D_i$  is the diameter of each elastomeric droplet, and  $N_i$  is the number of droplets with a diameter  $D_i$ . The standard deviation of the diameter distribution was 0.11  $\mu\text{m}$  for EOC-L materials and 0.47  $\mu\text{m}$  for EBC-H samples. The EOC-H compound plaques show a standard deviation of the diameter distribution of 0.37  $\mu\text{m}$ .

The distribution of the distances to the nearest neighbor was obtained using ImageJ software. It is important to remark that this distance was the edge to edge distance and was calculated measuring the distance for each particle to all neighbors and obtaining the minimum value.

The deformation of the particles was calculated following equation 9:

$$D = \frac{L-S}{L+S} \quad (9)$$

Where L and S are respectively the long and the short axis of each particle.

The average of the distributions of interparticle distance and deformation was calculated. The standard deviation of interparticle distance distribution varied between 0.1  $\mu\text{m}$  for low viscosity elastomer to 0.3  $\mu\text{m}$  for the high viscosity ones. Finally, the standard deviation for the deformation parameter was 0.15 for all the samples.

### ***Mechanical testing***

The notched Izod impact strength of the specimens was measured using a Frank 53566 Izod pendulum according to the UNE-EN ISO 180/A standard. The experiments were carried out at  $23 \pm 2^\circ\text{C}$  and  $50 \pm 10\%$  relative humidity according to the ISO 291 standard. The average value was obtained from testing seven specimens for each kind of material. The injection molded samples were machined to a size of 74 x 10 x 4 mm, removing the lateral skins of the samples before testing. The v-notch depth was 2 mm.

## **RESULTS AND DISCUSSION**

### **Properties of the blends**

#### ***Rheological characterization***



The complex viscosity of the pure materials was obtained performing frequency sweeps in the conditions previously mentioned (these data have been included in the supplementary information, Figure S1). The viscosity ratio  $p$  (equation 3) was calculated because of its influence on the elastomer morphology, as it was explained in the introduction (Figure 2):

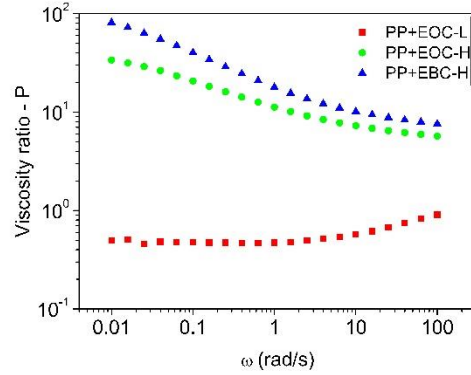


FIGURE 2. Calculated viscosity ratio (equation 3) for the blends.

The viscosity of the pure materials agrees with the measured melt flow index (indicated in the Materials section). The matrix viscosity is low, as would be expected for an injection grade (Figure S1 supplementary information). The only elastomer comparable in viscosity was EOC-L, obtaining a  $p$  ratio close to 1. The other two elastomers were more viscous, especially, the EBC-H. As a result, the  $p$  ratio was higher for these two materials (above 10).

The elastomer particle size was determined in the blends before the injection molding process, this is, right after the blending by extrusion. Some examples of SEM images are summarized in Figure 3.

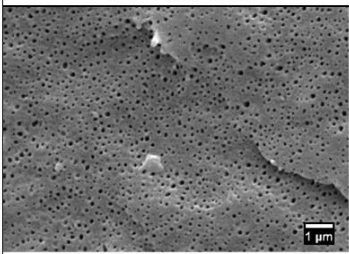
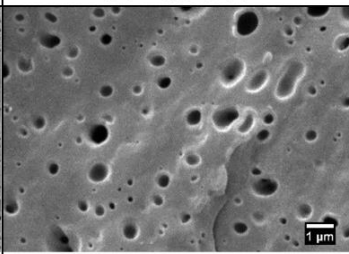
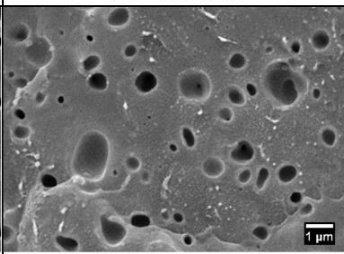
| MATERIALS BEFORE INJECTION MOULDING |   |  |   |
|-------------------------------------|---|--|---|
|                                     | PP+EOC-L  | PP+EOC-H   | PP+EBC-H  |
|                                     |  |  |  |
| $D_n$ ( $\mu\text{m}$ )             | 0.07  | 0.32   | 0.51  |
| $D_v$ ( $\mu\text{m}$ )             | 0.08  | 0.84   | 0.89  |

FIGURE 3. SEM images of xylene etched materials before injection molding. Scale bar represents 1  $\mu\text{m}$ .

The number and volumetric average diameters are indicated below the correspondent image.

The differences between the EOC-L blend and the other two materials are clearly observed. As expected, (equation 2), small particle size was achieved for the low viscosity material. Also, the slightly higher droplet diameter of EBC-H in comparison with EOC-H can be explained observing the viscosity ratio, higher for EBC-H. It should be noted that for  $p > 4$ , no breakup of droplets is expected in simple shear flow.<sup>17,38</sup>

Figure 4 shows the viscosity of the produced blends as a function of the frequency.

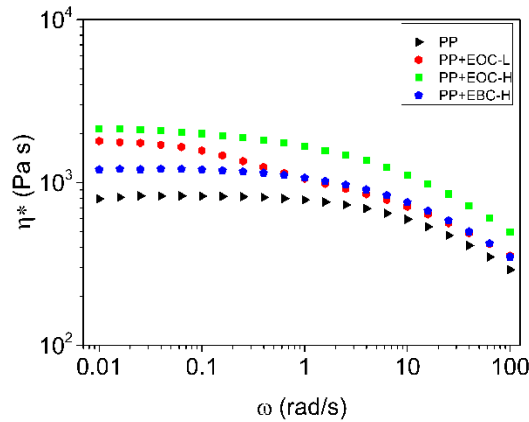


FIGURE 4. Complex viscosity of PP and PP/elastomer blends.

As expected, the material with a higher viscosity is the one including the EOC-H elastomer, followed by the PP+EOC-L and PP+EBC-H. On the other hand, the addition of EOC-L produces a blend more viscous than the sum of its components (Figure S2 of the supplementary information). Moreover, a shoulder appears for low frequencies. This is produced by a high interfacial adhesion in this system. This effect can be quantitatively confirmed by the analysis of the modulus. The storage modulus ( $G'$ ) of the components and the blends are included in figure 5. In addition, the logarithm mixing rule and the Palierne fitting are also included.

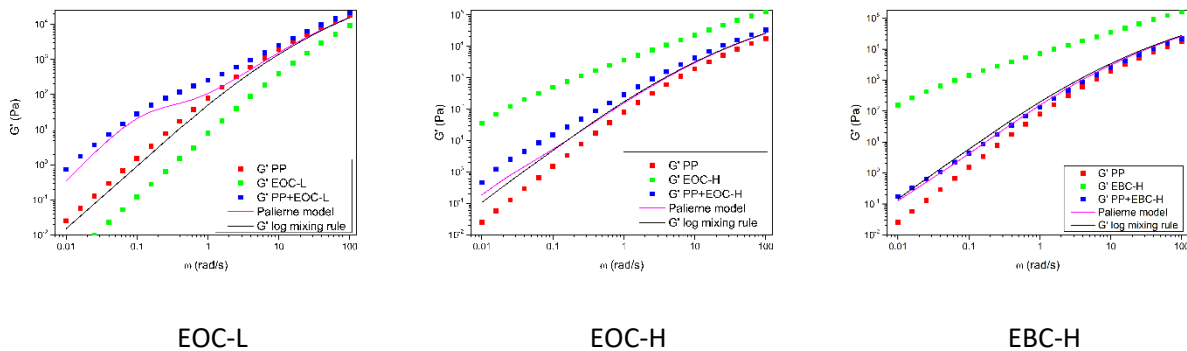


FIGURE 5. Storage modulus of pure components and their corresponding blends fitted using Log mixing rule model and Palierne model.

It can be noticed that at high frequencies, the experimental data and the logarithm mixing rule are very close. However, at low frequencies, trends are different for the various blends: For ECO-L material, a shoulder at low frequencies is shown. It was also observed, with lower intensity, in EOC-H blend. Finally, for EBC-H, the fitting to the mixing rule was very accurate along the frequency sweep. The apparition of a shoulder at low frequencies is widely known<sup>17</sup>. When dispersed phase droplets are slightly sheared, a

shaper relaxation process occurs, the interface being the source of an extra-elasticity. The model that incorporates this effect (Palierne model) showed the right trend for the EOC-L and EOC-H blends.

The interfacial tension was calculated from the Palierne model (Table 2), using the volumetric radius values from Figure 3. The coefficient of correlation  $R^2$  has also been included in the table, showing that the best fitting is for PP+EBC-H and the worst is for PP+EOC-H.

TABLE 2. Interfacial tension and determination coefficient for the Palierne model fitting

|          | $\sigma$ ( $\mu\text{N/m}$ ) | $R^2$  |
|----------|------------------------------|--------|
| PP+EOC-L | 50.60                        | 0.9608 |
| PP+EOC-H | 222.64                       | 0.9513 |
| PP+EBC-H | 251.37                       | 0.9979 |

The interfacial tension for the EOC-L was very low (5 times lower than for the other elastomers). Then, extremely high adhesion between phases is found for the EOC-L blend. On the other hand, EBC-H interfacial tension was the highest, expecting a lower bonding and a negligible role of the interphase in the properties of this material. Zhu performed experiments with the same EOC-H and a more viscous PP than the one used in this research, observing the same type of curves.<sup>39</sup> He obtained a value of 325  $\mu\text{N/m}$  from Palierne fitting at 210 °C and, being this value of the same order of magnitude than the value that has been obtained in our research (222.64  $\mu\text{N/m}$ ).

Values of the same order of magnitude were obtained for other conditions by Carriere (560  $\mu\text{N/m}$ ), Kontopoulou (600  $\mu\text{N/m}$ ), and Zhang (670  $\mu\text{N/m}$ ).<sup>40-42</sup> The low viscosity of the PP likely caused the lower values obtained in our study in comparison with the ones found in the literature

The values of  $R^2$  were smaller for EOC compounds compared with the one obtained for EBC compound. The reason could be partial miscibility. The Palierne model was developed for immiscible blends. Possible partial miscibility of octene-ethylene copolymers (especially EOC-L) could cause a deviation of the experimental data and the predictions of the model.<sup>43</sup> Miscibility of these type of elastomers in PP has been previously reported in the literature, but in our case, only the elastomers with octene seemed to be partially miscible.<sup>41, 44</sup>

### **Calorimetric characterization**

The melting curves in the first and second heating cycle and the crystallization curves of PP and PP/elastomer blends are displayed figure 6. The critical points (Melting temperature  $T_m$ , the temperature of the onset of crystallization  $T_c^{onset}$  and peak crystallization temperature  $T_c^{peak}$ ) are collected in Table 3. The PP phase's crystallinity is also included.

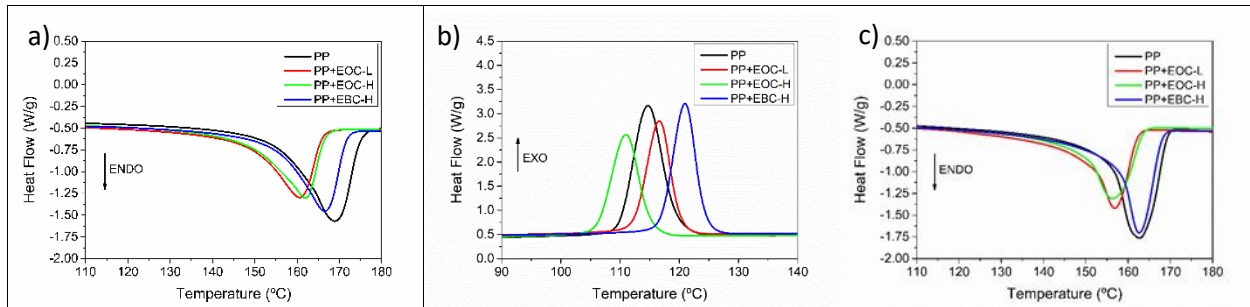


FIGURE 6. a) First heating, b) cooling segment and c) second heating cycles in DSC experiments at 10 °C/min.

TABLE 3. Crystallinity of the PP phase and melting and crystallization temperatures of the blends

|          | First Heating   |            | Cooling            |                   | Second Heating  |            |
|----------|-----------------|------------|--------------------|-------------------|-----------------|------------|
|          | $\chi_{PP}$ (%) | $T_m$ (°C) | $T_c^{onset}$ (°C) | $T_c^{peak}$ (°C) | $\chi_{PP}$ (%) | $T_m$ (°C) |
| PP       | 48.9            | 168.95     | 127.2              | 114.9             | 54.9            | 162.7      |
| PP+EOC-L | 43.4            | 160.5      | 126.1              | 116.9             | 47.5            | 156.9      |
| PP+EOC-H | 42.6            | 162.2      | 124.2              | 111.1             | 47.0            | 156.2      |
| PP+EBC-H | 45.6            | 166.55     | 130.0              | 121.1             | 52.4            | 162.5      |

In the first heating (Figure 6 a)), the obtained information is related to the morphology obtained after extrusion process. On the other hand, the second heating cycle (Figure 6 c)) provides information about the crystalline morphology after the controlled cooling and crystallization segment, that is included in Figure 6 b). Then, the general crystallization and melting trends of these materials can be deduced from Figure 6.

The curves showed the typical melting and crystallization shape for PP and blends under DSC controlled conditions, as can be seen in Ying study.<sup>45</sup> Two different melting behaviors for the studied materials were observed in both of the cycles (trends are the same for both heating cycles): On one hand, a high melting temperature for PP and PP+EBC-H (in the range of 167-169 °C in the first heating and 162 °C in the second heating), that correspond with a well-formed and larger crystalline morphology, with higher crystallinity; and on the other hand, a lower melting temperature (close to 161 °C in the first heating and 156 °C in the second heating) and lower crystallinity for EOC compounds. The difference in melting temperature (approximately 6-7 °C) is likely due to the partial miscibility of the elastomers' chains in PP for EOC. This result confirms the previous analysis of the rheological data.

There are also clear differences in the crystallization behavior. Figure 6 b) shows the highest crystallization temperature peak for PP+EBC-H compound, whereas PP+EOC-H was the material with the lowest crystallization temperature peak. PP and PP+EOC-L crystallization peaks were between the other two. To

analyze these data in more detail, the relative crystallinity during crystallization as function of time has been calculated (Figure 7):<sup>45</sup>

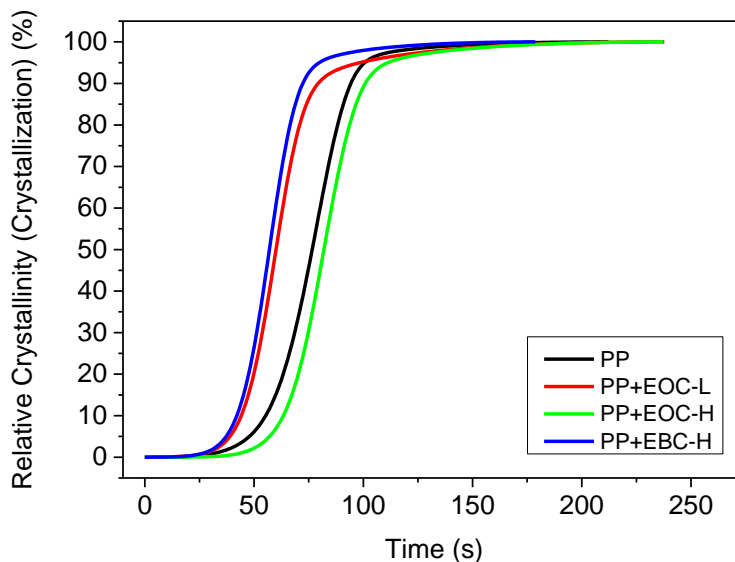


FIGURE 7. Relative crystallinity curves as a function of time.

Two different behaviors can be distinguished: Fast crystallization for EBC-H and EOC-L compounds (that are the more and less viscous polymers respectively) and slower crystallization for pure PP and EOC-H compound. The explanation for this behavior and relation with miscibility is as follows:

- Well separated phases of EOC-H elastomer in PP produced heterogeneous nucleation of PP crystals, being the crystallization peak temperature the highest observed and the crystallization kinetics the fastest, enhancing the crystallinity degree.
- EOC elastomers were partially miscible in PP, but the effect over crystallization was different, depending on the viscosity: Low viscous materials are formed of short chains (low molecular weight), whose crystallization is faster than that of long chains (high molecular weight). Therefore, it is expected that the miscible EOC-L chains could boost PP crystallization and EOC-H act in the opposite direction. So, both were partially miscible and decreased the crystallinity of PP phase, but the crystallization rate in EOC-L compound was higher.

Ying studied the PP-EOC non-isothermal crystallization using the same EOC-H elastomer.<sup>45</sup> He also observed the previously mentioned reduction of melting temperature due to PP-EOC interaction. For small percentages of elastomer (5-10 wt.%) the heterogeneous crystallization speeded up the crystallization, but for higher percentages the crystallization time was increased due to the strong intermolecular interaction and chain entanglements. In our case, the same interpretation was valid, but EOC-L could not hinder the crystallization with the same intensity (few chain entanglements due to low molecular weight) and favor a faster crystallization than EOC-H.

## Structure and properties of the injection molded samples

### *Elastomer morphology*

Following the existing studies about injection molded samples composed by PP-elastomer blends, the MD-Z plane was characterized by a hierarchical structure.<sup>21-23</sup> Following these studies, images taken from the skin to the center in the MD-Z plane should provide three different layers:

- A skin, produced by the dynamic flow and the PP crystallization, that rejects the elastomer particles to the core.
- A shear layer, in which the particles are elongated due to the high shear rates
- A core layer, in which spherical droplets predominate, with the possibility of coarsening phenomena.

Figure 8 shows representative SEM micrographs of the produced solid and foamed samples. SEM images were taken at 50, 100, 200, 500, 1000 and 2000  $\mu\text{m}$  from skin, the last image matching with the center of the sample.

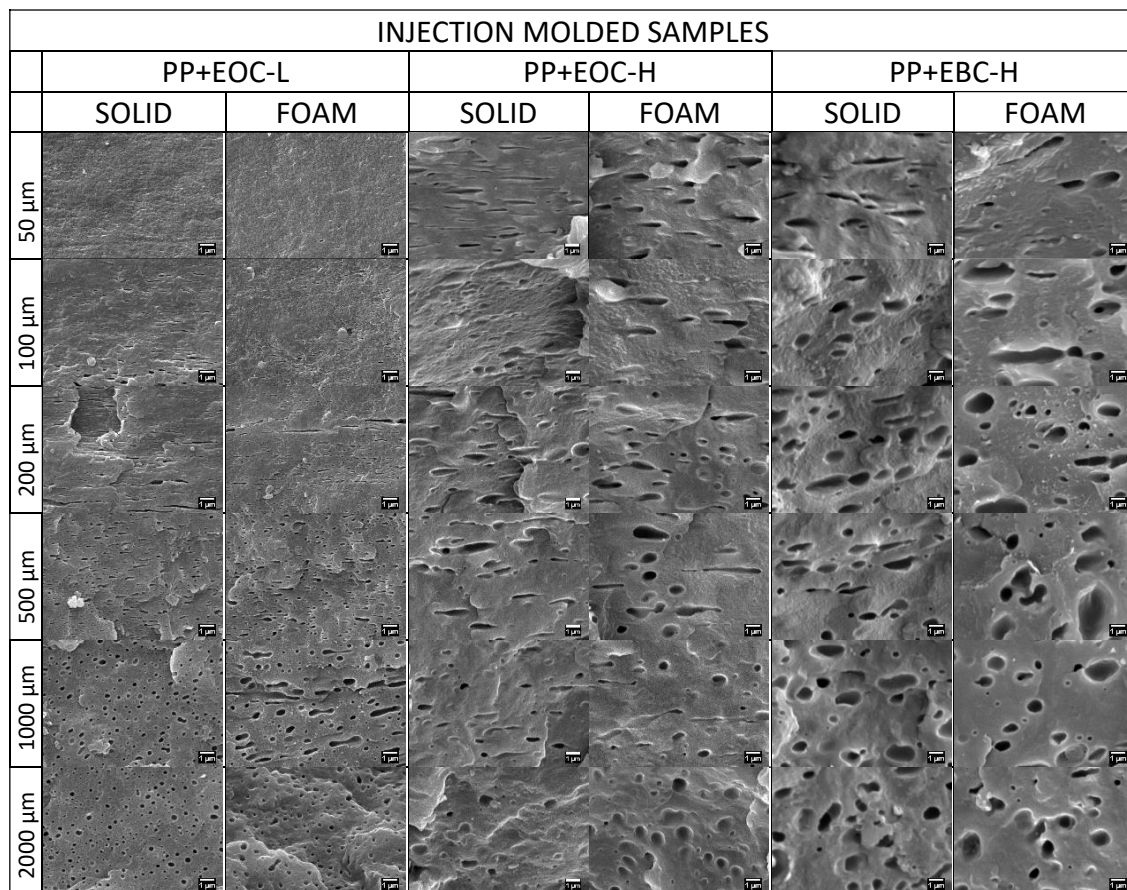


FIGURE 8. SEM images of xylene etched solids and foams for different distances from the injection molded sample's skin. In the core of the foam, images were taken in the interior of the walls. The scale bar represents 1  $\mu\text{m}$ .

There are apparent differences between the samples. For a better comparison and adequate analysis, the droplet diameter, interparticle distance, and deformation of the particles were measured (figure 9).

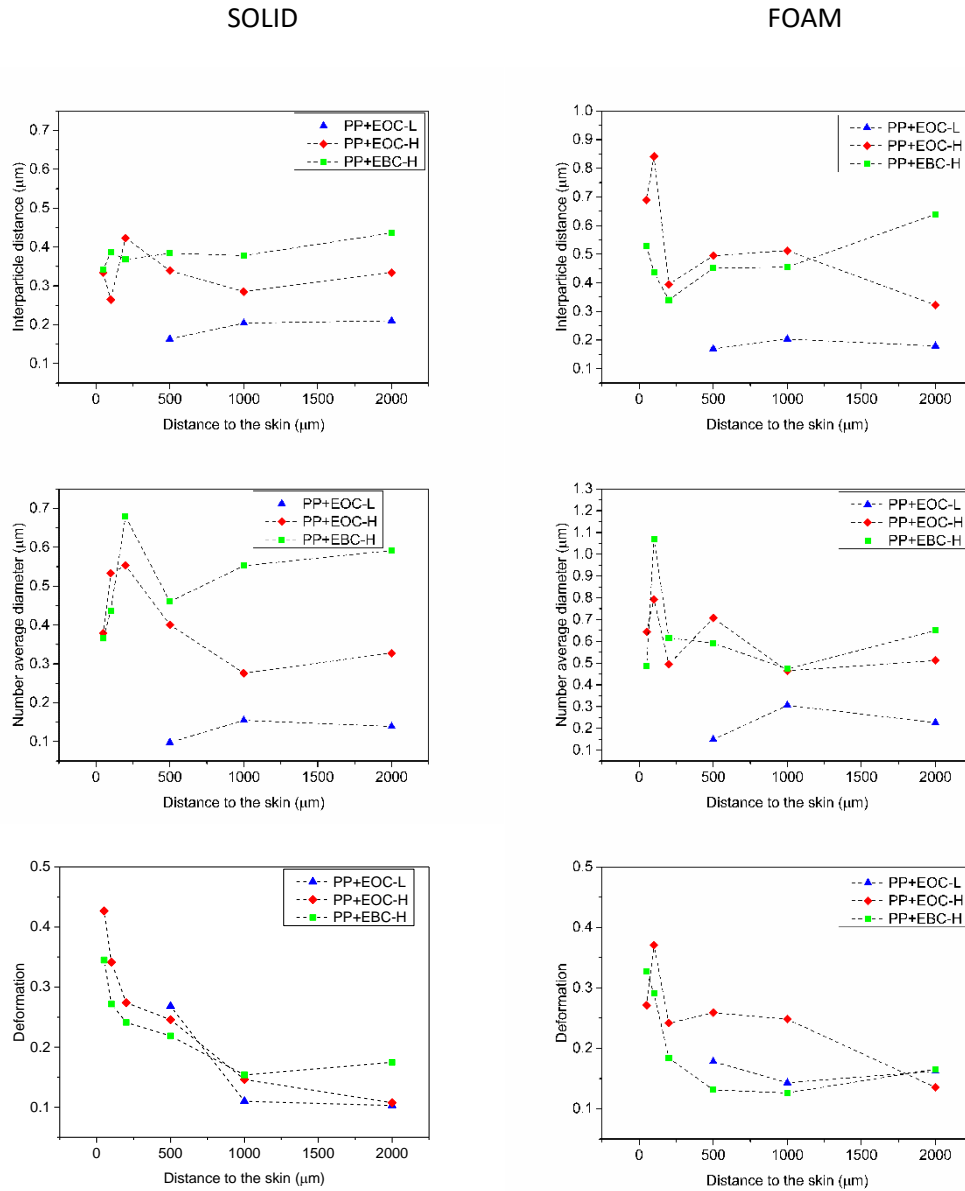


FIGURE 9. Interparticle distance, number average diameter and deformation for solid and foamed samples.

Several conclusions can be extracted from the obtained data:

- An elastomer free skin layer was only present in PP+EOC-L blends (both solid and foamed). This skin layer showed a thickness of around 500 µm.
- The lower diameter and interparticle distance were reached for EOC-L compound both for solid and foams, which agrees with the data for the blended compounds diameter (Figure 3).

- However, if the diameter of the material before injection (Figure 3) is compared with the diameter after injection molding, a larger increment in the particle size occurred for EOC-L compound.
- In foamed materials, the diameter and the interparticle distance reached superior values than for the same solids, suggesting the existence of coarsening during foaming injection molding.
- Deformation was higher near the skins, indicating the existence of the shear layer. The values are lower in the core layer. In foams, deformation is lower in the shear layer compared with the solids.

The differences observed in elastomer morphology can be explained using the rheological characterization. The  $p$  ratio was smaller for the PP+EOC-L the blend. A low  $p$  value is associated to a higher deformability of the droplet because a lower shear rate is necessary to exceed  $Ca_{crit}$ . The small radius ( $R$ ) of this blend (Figure 3) should increase the droplet resistance to be deformed, but the very low  $\sigma$  (Table 2) counteracts this effect. Then, being necessary a low shear rate to deform the droplets, it seemed plausible the coarsening of the droplets in this blend due to shear coalescence. Then, the low viscosity ratio  $p$  in EOC-L blend explained the existence of coalescence in that compound. On the other hand, the other two compounds, with higher  $p$  have not suffered such increase in their elastomer particle size in comparison with the blends before injection molding.

The free-elastomer skin in PP+EOC-L solid and foamed injected samples could also be related to  $p$ . Ying explained this type of skin in PP/EOC injected samples based on crystalline rejection and flow.<sup>21</sup> It seemed more plausible that the crystalline front rejects small low viscous particles than large size viscous particles. Following this reasoning, high viscosity elastomer compounds showed elastomer droplets near the skin.

The elastomer morphology in foams is also conditioned, as it was proved in a previous study,<sup>34</sup> by the lower viscosity of the materials after including the gas phase,<sup>46</sup> and their higher thermal insulation capability. In the first case, the lower shear rate deformed less the droplets, showing lower deformation in the shear layer. The higher thermal insulation caused that the temperature was higher in the foams core than in the corresponding solids. The dependence of coalescence and Ostwald ripening in quiescent melt polymer blends with temperature is well known.<sup>47, 48</sup> A slow cooling of the sample can imply a boosting of morphology degeneration due to these effects. As a consequence, a larger particle size is achieved in the core of cellular polymers.

### ***Analysis of the cellular structure***

Examples of SEM images of the TD-Z plane of the foamed samples are collected in Figure 10, and the cell size, normalized standard deviation of the cellular structure and skin thickness are summarized in Table 4:



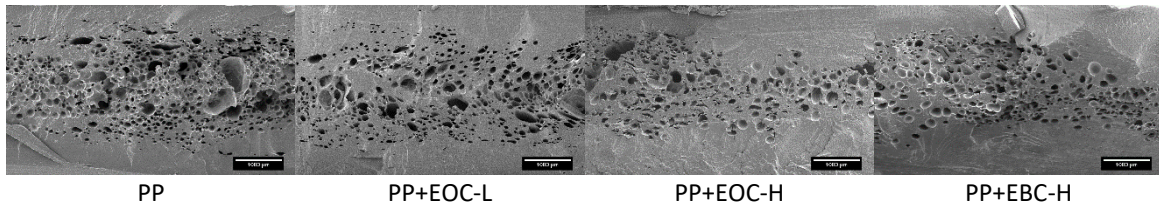


FIGURE 10. SEM images of the TD plane of foams for the different used compounds. The scale bar represents 1 mm.

TABLE 4. Cell size, standard deviation of the cell size distribution and skin thickness of foamed samples

|          | $\phi_{3D}(\mu\text{m})$ | SD/ $\phi$ | Skin (%) |
|----------|--------------------------|------------|----------|
| PP       | 120.46                   | 0.71       | 29.37    |
| PP+EOC-L | 149.11                   | 0.65       | 34.54    |
| PP+EOC-H | 99.35                    | 0.74       | 50.89    |
| PP+EBC-H | 101.47                   | 0.73       | 43.82    |

All the materials showed a closed cell cellular structure (this result was confirmed by using gas pycnometry). Comparing the different references, the materials with low viscosity (PP and PP+EOC-L) were characterized by large voids and small cells, which increase the average cell size of these materials. These structures are common in foams obtained by low-pressure injection molding process, characterized by a low uniformity.<sup>48</sup> However, it seems clear that the viscosity of the material played an important role. The presence of smaller cells can be related to a more controlled cell growth when the blend's viscosity is high, as in the case of EOC-H and EBC-H compounds.<sup>49</sup> On the other hand, a low melt viscosity caused structure degeneration. The reason is that low viscosity increased the rate of melt drainage, reduces surface tension and increases the critical radius of a cell to be stable.<sup>50</sup>

A higher skin thickness was observed in the two materials with higher viscosity. This parameter strongly depends on the crystallization temperature. The mold walls are cold, and the fast crystallization avoid the development of a cellular structure. Then, the polymer with a higher crystallization temperature should show a thicker solid skin. However, in our case, the EOC-H and EBC-H compounds were characterized by a skin thickness higher than 40%. This result indicated a link between skin thickness and viscosity. The high viscosity could avoid cells' growth before the crystallization, being this effect more important than the differences in the crystallization behavior.

### ***Mechanical properties***

The obtained values of the notched Izod impact test for the solid and foamed samples are summarized in Figure 11. The type of failure (C = Complete break and H = Hinge break) is also indicated.

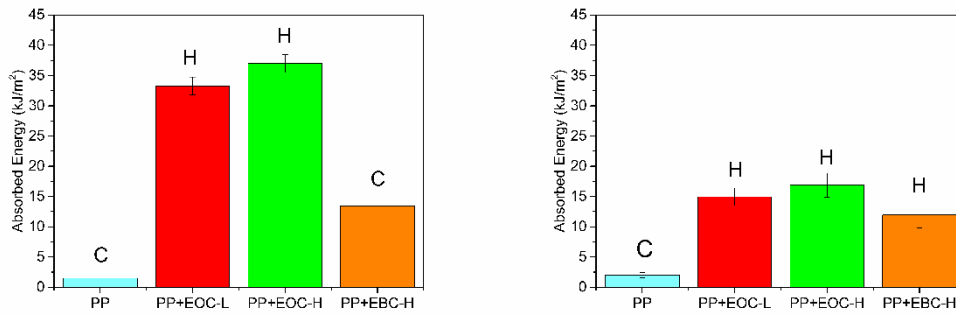


FIGURE 11. Absorbed energy in Izod impact test for solid (left) and foamed samples (right). The letter indicates the type of failure (Hinge (H) or complete (C) break)

Firstly, a dependence with the use of elastomer and the type of elastomer can be appreciated for the solids (non-foamed materials). The addition of elastomer produced an increment of absorbed energy of 9 times in the worst of the cases and of 25 times in the best case in comparison with the raw PP sample, which behaved as a brittle material. The other aspect that is remarkable is the differences between the different elastomers. The EOC elastomers, and specially the higher viscosity grade, showed higher values than EBC compound. Moreover, the type of failure is hinge break for EOC, against the complete break observed in EBC-H compound.

After foaming, the order of reinforcement between elastomer types is maintained. However, a higher relative decrease in energy between solid and foams can be observed for the more ductile solids. The decrease for EBC-H compound was about 13%, a very low reduction compared with the one observed in the other elastomer compounds (about 55% of reduction). Furthermore, the EBC-H materials showed a hinge break, changing with respect to the solid samples based on this blend. Despite this large reduction, using the scale laws (Eq. 4), the  $n$  exponent was about 2.9 for both EOC blends, that indicates that the absorbed energy was better than expected, taking into account that the expected values for  $n$  are between 3 and 4.<sup>29,30</sup> Finally, PP increased its impact resistance when it was foamed: the absorbed energy of the foamed PP was 33% higher than that of the solid parts.

We have analyzed the relation between the microstructure observed in figures 9 and 10 and the absorbed energy in the Izod test in both solids and foams. On the one hand, EOC-H compound interparticle distance was much higher than the one obtained for EOC-L blend (Figure 10) and the impact resistance was slightly better, contradicting the interparticle distance model.<sup>12</sup> The high viscosity compounds (EOC-H and EBC-H) exhibited similar elastomer morphology and, however, the absorbed energy was 60% lower for the last blend.

Firstly, taking into account figure 2 and 3, it was clear the relation between viscosity and the microstructure of the sample. Also, it is known the importance of interparticle distance in impact response of polymer blends.<sup>13</sup> A study that reached this conclusion was carried out by D'orazio,<sup>51</sup> determining that the viscosity ratio ( $p$ ) sets the interparticle distance and predetermine the impact behavior, However, several studies using an elastomeric dispersed phase with different viscosities has perceived that interparticle distance was not so crucial, as Wu's model determined.

For example, Oshinski studied the impact behavior of several nylon and SEBS blends, finding the relation with the viscosity of the matrix, but affirmed that the differences between the elastomers required more studies.<sup>52</sup> Other example was given by Yokoyama, that produced blends of PP with EBC and EOC elastomers.<sup>9</sup> When a high viscosity elastomer was used, the domains increased their size, and then, the interparticle distance raises. However, the absorbed energy increased too, contradicting the Wu's model. He affirmed that molecular weight and chemical nature of the rubber surpassed the effect of morphology. Also, Rabinovitch confirmed that, despite the claims in literature about the improvement of impact resistance when small rubber particles characterize the blend, he observed that low viscosity EOC particles in PP did not reach the efficiency of high viscosity EOC ones.<sup>27</sup> Then, in the reviewed cases, molecular weight of the elastomer or the chemical interaction weighted more than the obtained morphology. This is the same behavior we have observed in our materials, both for solids and foamed materials, viscosity of the elastomeric phase is playing a key role.

In addition, the adhesion between phases is also important. This parameter was stronger in EOC-L and lower in EBC-H (Figure 4, 5 and table 2). The low adhesion between EBC-H elastomer and PP phase can avoid the adequate transmission of the deformation during impact. Then, the absorbed energy due to the rubber cavitation did not improve the toughness in a significant way for this particular blend

In foams, the observed trends are similar than that found for the solids indicating that both viscosity and interfacial adhesion are also playing a major role on the impact performance. It is interesting to mention that the lower reduction of absorbed energy for EBC-H compound could be explained in the same way that the improvement of PP when it was foamed. It can be seen that the lower the ductility (or higher the brittleness) of the solid, a better relative impact resistance was obtained. This makes sense because a brittle material cannot lose much more absorbed energy when it is foamed, because the solid material performed poorly. Moreover, foaming in EBC-H compound seemed to improve the failure of impacted samples. It could be attributed to the obtained cellular structure's quality, characterized by a low cell size and thick solid skins.

In addition, for EOC compounds, the obtained foams showed an adequate cellular structure: both of them showed a considerable amount of solid skin (especially in EOC-H case) and the average cell size, was similar to that of the pure PP. This allowed obtaining a good impact response, reducing the effect of the ductile-brittle transition. This is confirmed by analyzing the  $n$ -exponent,  $n=2.9$ , lower than the expected value ( $n$  between 3 and 4). Therefore, and for these materials, elastomer toughening was a good strategy to improve the energy absorbed by foams, being the EOC elastomer with a higher viscosity (EOC-H) the optimum one because provides a solid phase with an adequate morphology and properties and a thick solid skin and reduced cell sizes.

## **CONCLUSIONS**

Elastomers with different viscosities (high and low) and chemical composition (EOC and EBC) were blended with PP in order to improve the impact behavior of solids and cellular polymers produced by injection molding. The content of elastomer in all blends was 20%wt.

The interphase between the phases of the blends composed by EOC elastomers was stronger, especially in the low viscosity EOC blend. Calorimetric techniques confirmed the existence of partial miscibility of EOC in PP. Moreover, the rheological studies predicted the elastomer morphology in foams and solids. The key parameter was the viscosity ratio between the dispersed phase and the matrix, obtaining smaller particles for the elastomer with a lower viscosity (EOC-L). Foaming affects the elastomer morphology, being the elastomeric particles larger and more separated in the cellular polymers.

Cellular structure was also related with the blends viscosity, degeneration., The blends with higher viscosities EOC-H and EBC-H showed an improved cellular structure characterized by smaller cells sizes and thicker skin.

The impact behavior of injected molded solids and foams was determined. Elastomer toughening in solids was achieved for EOC compounds, and to a lesser extent for EBC. The results obtained indicate that viscosity of the elastomeric phase and adhesion between phases are the key parameters controlling the impact behavior of the samples under study. , being the EOC-H blend the optimum material because combines a high viscosity with and adequate adhesion between phases.

The results for the cellular polymers showed similar trends to those of the solids showing that viscosity and interfacial adhesion are also playing a major role on the properties of the foamed samples. In addition, we have found that the expected reduction of the impact response when the materials are foamed, but for the EOC blends the  $n$  exponent in the scaling law relation was low (2.9) in comparison with the expected values (between 3 and 4). The EOC-H blend shows the most promising behavior due to a proper combination of polymer and elastomer morphology, large skin thickness and low cell size. The high viscosity of the elastomeric phase improves the mechanical behavior of the solid matrix and, in addition, improves the foaming behavior of the material, giving as a result an optimum cellular structure.

## ACKNOWLEDGEMENTS

Financial support from Junta of Castile and Leon grant (S. Muñoz-Pascual), Financial assistance from the Junta of Castile and Leon (VA275P18) and Spanish Ministry of Science, Innovation and Universities (RTI2018-098749-B-I00) is gratefully acknowledged. Financial support for the PhD students Mobility of University of Valladolid (2019) is also gratefully acknowledged.

## REFERENCES AND NOTES

1. Ma, L.F.; Wang, W.K.; Bao, R.Y.; Yang, W.; Xie, B.H.; Yang, M.B. *Mater. Des.* **2013**, *51*, 536–543.
2. Sharma, R.; Maiti, S. N. *Polym Plast Technol Eng.* **2014**, *53*(3), 229-238.
3. Fanegas, N.; Gómez, M. A.; Jiménez, I.; Marco, C.; Garcia-Martínez, J. M.; Ellis, G. *Polym. Eng. Sci.* **2008**, *48*(1), 80-87.
4. Mae, H.; Omiya, M.; Kishimoto, K. *J. Appl. Polym. Sci.* **2008**, *107*(6), 3520-3528.
5. Zebarjad, S. M.; Bagheri, R.; Reihani, S. M.; Lazzeri, A. *J. Appl. Polym. Sci.* **2003**, *90*(14), 3767-3779.

6. Doshev, P.; Lach, R.; Lohse, G.; Heuvelsland, A.; Grellmann, W.; Radusch, H. J. *Polymer* **2005**, *46*(22), 9411-9422.
7. Keskin, R.; Adanur, S. *Polym Plast Technol Eng.* **2011**, *50*(1), 20-28.
8. Lim, J. W.; Hassan, A.; Rahmat, A. R.; Wahit, M. U. *J. Appl. Polym. Sci.* **2006**, *99*(6), 3441-3450.
9. Yokoyama, Y.; Ricco, T. *Polymer* **1998**, *39*(16), 3675-3681.
10. Kontopoulou, M.; Wang, W.; Gopakumar, T. G.; Cheung, C. *Polymer* **2003**, *44*(24), 7495-7504.
11. Sun, D. X.; Lei, Y. Z.; Lu, Y.; Cao, S.; Qi, X. D.; Wang, Y. *Compos. Sci. Technol.* **2020**, 108148.
12. Wang, J.; Zhang, X.; Jiang, L.; Qiao, J. *Prog. Polym. Sci.* **2019**, 101160.
13. Wu, S. *J. Appl. Polym. Sci.* **1988**, *35*(2), 549-561.
14. Jiang, W.; Tjong, S. C.; Li, R. K. Y. *Polymer* **2000**, *41*(9), 3479-3482.
15. Fasihi, M.; Mansouri, H. *J. Appl. Polym. Sci.* **2016**, *133*(40).
16. Premphet, K.; Paecharoenchai, W. *J. Appl. Polym. Sci.* **2002**, *85*(11), 2412-2418.
17. Tucker III, C. L.; Moldenaers, P. *Annu Rev Fluid Mech.* **2002**, *34*(1), 177-210.
18. Wu, S. *Polym. Eng. Sci.* **1987**, *27*(5), 335-343.
19. Shariatpanahi, H.; Nazokdast, H.; Dabir, B.; Sadaghiani, K.; Hemmati, M. *J. Appl. Polym. Sci.* **2002**, *86*(12), 3148-3159.
20. Tokita, N. *Rubber Chem. Technol.* **1997**, *50*(2), 292-300.
21. Ying, J.; Xie, X.; Peng, S.; Zhou, H.; Li, D. *J. Thermoplast. Compos. Mater.* **2018**, *31*(9), 1263-1280.
22. Li, J.; Zhang, X.; Qu, C.; Zhang, Q.; Du, R.; Fu, Q. *J. Appl. Polym. Sci.* **2007**, *105*(4), 2252-2259.
23. Liu, F.; Zhang, Y.; Zhang, Y.; Huang, Z.; Ying, J.; Xie, X.; Zhou, H. *Adv. Polym. Tech.* **2017**, *36*(3), 341-351.
24. Koning, C.; Van Duin, M.; Pagnoulle, C.; Jerome, R. *Prog. Polym. Sci.* **1998**, *23*(4), 707-757.
25. Yu, Z. Z.; Ou, Y. C.; Hu, G. H. *J. Appl. Polym. Sci.* **1998**, *69*(9), 1711-1718.
26. Wahit, M. U.; Hassan, A.; Mohd Ishak, Z.; Czigány, T. *Express Polym Lett.* **2009**, *3*(5), 309-319.
27. Rabinovitch, E. B.; Summers, J. W.; Smith, G. J. *Vinyl Addit. Technol.*, **2003**, *9*(2), 90-95.
28. Klemperer D.; Frisch, K.C. Handbook of polymeric foams and foam technology. Hanser: Munich, Germany, **1991**.
29. Tejada, E. H.; Sahagún, C. Z.; González-Núñez, R.; Rodrigue, D. *J. Cell. Plast.* **2005**, *41*(5), 417-435.
30. Throne, J. L.; Progelhof, R. C.; Kumar, S. *J. Cell. Plast.* **1985**, *21*(2), 123-140.
31. Gong, W.; Fu, H.; Zhang, C.; Ban, D.; Yin, X.; He, Y.; Pei, X. *Polymers* **2018**, *10*(12), 1375.
32. Heidari, A.; Fasihi, M. *Express Polym. Lett.* **2019**, *13*(5), 429-442.

33. Zhao, J.; Zhao, Q.; Wang, G.; Wang, C.; Park, C. B. *Macromol. Mater. Eng.* **2020**, *305*(1), 1900630.
34. Muñoz-Pascual, S.; Lopez-Gonzalez, E.; Saiz-Arroyo, C.; Rodriguez-Perez, M. A.; *Polymers* **2019**, *11*(5), 894.
35. Shutov, F. A. Integral structural polymer foams: technology, properties and applications. Springer Science & Business Media: Berlin, Germany, **1986**.
36. Ahmed, A. K.; Atiqullah, M.; Pradhan, D. R.; Al-Harathi, M. A. *RSC Adv.* **2017**, *7*(67), 42491-42504.
37. Pinto, J.; Solórzano, E.; Rodriguez-Perez, M. A.; de Saja, J. A. *J. Cell. Plast.* **2013**, *49*(6), 555-575.
38. Bruijn, de, R. A. Deformation and breakup of drops in simple shear flows. PhD thesis. Technische Universiteit Eindhoven. Eindhoven. Netherlands, **1989**.
39. Zhu, L.; Xu, X.; Ye, N.; Song, N.; Sheng, *Polym. Compos.* **2010**, *31*(1), 105-113.
40. Carriere, C. J.; Silvis, H. C. *J. Appl. Polym. Sci.*, **1997**, *66*(6), 1175-1181.
41. Kontopoulou, M.; Wang, W.; Gopakumar, T. G.; & Cheung, C. *Polymer*, **2003**, *44*(24), 7495-7504.
42. Zhang, Z.; Yu, F.; Zhang, H. *Polymers*, **2017**, *9*(6), 236.
43. Kwon, M. K.; Cho, K. S. *Korea-Aust. Rheol. J.*, **2016**, *28*(1), 23-31.
44. McNally, T.; McShane, P.; Nally, G. M.; Murphy, W. R.; Cook, M.; Miller, A. *Polymer* **2002**, *43*(13), 3785-3793.
45. Ying, J.; Liu, S.; Guo, F.; Zhou, X.; Xie, X. *J. Therm. Anal. Calorim.*, **2008**, *91*(3), 723-731.
46. Qin, X.; Thompson, M. R.; Hrymak, A. N. *Polym. Eng. Sci.* **2007**, *47*(4), 522-529. Crist, B.; Hill, M. J. *J. Polym. Sci. Pol. Phys.*, **1997**, *35*(14), 2329-2353.
47. Fortelný, I.; Živný, A.; Jůza, J. *J. Polym. Sci. Pol. Phys.*, *37*(3), **1999**, 181-187.
48. Lee, S. M. Handbook of composite reinforcements. John Wiley & Sons: Hoboken, NJ, USA, **1992**.
49. Song, Z. L.; Ma, L. Q.; Wu, Z. J.; He, D. P. *J. Mater. Sci.*, **2000**, *35*(1), 15-20.
50. Kadoi, K.; Nakae, H. *Mater. Trans.*, **2011**, 1108221452-1108221452.
51. D'orazio, L.; Mancarella, C.; Martuscelli, E.; Sticotti, G.; Massari, P. *Polymer*, **1993**, *34*(17), 3671-3681.
52. Oshinski, A. J.; Keskkula, H.; Paul, D. R. *Polymer*, **1996**, *37*(22), 4909-4918.